Microfluid Nanofluid
DOI 10.1007/s10404-013-1185-x

RESEARCH PAPER

Electrokinetic flow in a pH-regulated, cylindrical nanochannel containing multiple ionic species

Shiojenn Tseng · Yi-Hsuan Tai · Jyh-Ping Hsu

Received: 31 January 2013 / Accepted: 3 April 2013

Abstract Considering the wide applications of the electrokinetic flow regulated by pH, we model the flow of an electrolyte solution containing multiple ionic species in a charge-regulated cylindrical nanochannel. This extends previous analyses, where only two kinds of ionic species are usually considered, and a charged surface assumed to maintain at either constant potential or constant charge density, to a case closer to reality. Adopting a fused silica channel containing an aqueous NaCl background salt solution with its pH adjusted by HCl and NaOH as an example, we show that if the density of the functional groups on the channel surface increases (decreases), it approaches a constant potential (charge density) surface; if that density is low, the channel behavior is similar to that of a constant charge density channel at high salt concentration and large channel radius. Several interesting results are observed, for example, the volumetric flow rate of a small channel has a local maximum as salt concentration varies, which is not seen in a constant potential or charge density channel.

Keywords Electrokinetic flow · pH-regulated cylindrical nanochannel · Multiple ionic species

S. Tseng
Department of Mathematics, Tamkang University, Tamsui, Taipei 25137, Taiwan

Y.-H. Tai · J.-P. Hsu (✉)
Department of Chemical Engineering, National Taiwan University, Taipei 10617, Taiwan
e-mail: jphsu@ntu.edu.tw

1 Introduction

Electrokinetic flow has been applied extensively in separation devices, micropumps, and biochemomedical analyses (Daiguji et al. 2004a, b; Mei et al. 2008; Karenga and El Rassi 2010; Karnik et al. 2005; Wang et al. 2009). The fast advances in micro- and nano-scaled channel (Gasparac et al. 2004; Tas et al. 2002; Campbell et al. 2004; Mao and Han 2005) and pore (Li et al. 2001; Storm et al. 2003; Krapf et al. 2006) fabrication techniques make it highly necessary to establish a general theoretical approach for the analysis of the associated electrokinetic phenomena such as electroosmotic flow. For a narrow channel, since the thickness of electrical double layer (EDL) can be comparable with its radius, EDL overlapping might occur, yielding several interesting phenomena, such as ion enrichment (Pu et al. 2004) and concentration polarization (Kim et al. 2007; Nischang et al. 2006). As pointed out by Schoch et al. (2006), due to EDL overlapping, the behavior of the electroosmotic flow in a nanochannel deviates appreciably from that in a microchannel.

Both the direction and the magnitude of the electroosmotic flow in a narrow channel can affect strongly the associated applications; both of them depend upon its charged conditions, the strength of the applied electrical field and the physicochemical properties of the liquid phase. In practice, many narrow channels have ionizable functional groups and, therefore, are charged when in contact with liquid such as water. For example, pure silica channels have silanol groups (Nawrocki 1997; Liu and Maciel 1996), and titanium oxide (Hirst et al. 2005) channels bring hydroxide groups. When immersed in an aqueous environment, these functional groups dissociate or absorb ions, yielding a channel charged. In these cases, because the charged conditions depend upon the solution

Published online: 14 April 2013

properties such as its pH and the background electrolyte concentration, they are referred to as charge-regulated surface (Hu and Bard 1997; Yeh et al. 2012a, b). This nature, however, is often neglected in relevant studies, for simplicity, and a charged surface is usually assumed to maintain at either a constant electrical potential (Ai et al. 2010; Pennathur and Santiago 2005) or constant charge density (Qiao and Aluru 2004; Wang et al. 2007; White and Bund 2008). Note that these two idealized conditions are the limiting cases of a charge-regulated surface.

The solution pH is usually adjusted by introducing reagents such as HCl and NaOH for various purposes. Due to the presence of background salts and/or buffer, this implies that besides the ionic species coming from those salts, the presence of other ionic species can be significant. For example, if solution pH deviates appreciably from 7, the presence of H^+ or OH^- might be significant. In addition, the solution pH is often an important factor to the charged conditions of a charge-regulated surface. For simplicity, previous studies in electrokinetic phenomena almost always assumed that the ionic species in the liquid phase come mainly from the background salt, and only two kinds of ionic species are taken into account (Yuan et al. 2007; van der Heyden et al. 2005; Wang et al. 2010).

The above discussions suggest that extending previous analyses on electrokinetic flow to the case where the charged conditions on the channel wall depend upon solution conditions taking account of the presence of multiple ionic species is highly desirable. This is done in the present work by considering a fused silica channel of radius ranging from 50 to 500 nm containing an aqueous NaCl (background salt) solution with its pH adjusted by HCl and NaOH as an example. Because the length scale of solvent molecules is much smaller than that of the channel, a continuum model (Qu and Li 2000; Daiguji et al. 2004a, b) is applied, instead of a model based on molecular scale (Thompson 2003; Cao et al. 2010). The channel surface can assume an arbitrary level of electrical potential, which is desirable in practice. In addition to verifying the applicability of the model proposed by the available experimental data in the literature, a thorough numerical simulation is conducted to examine the influences of solution pH, background salt concentration, density of ionizable functional groups on the channel surface, and the channel radius on the volumetric flow rate and velocity distribution. The results gathered provide a useful guideline for experimentalists both to explain their data and to design electrokinetic devices.

2 Theory

As shown in Fig. 1, we consider the electrokinetic flow along the axis of a cylindrical nanochannel of radius

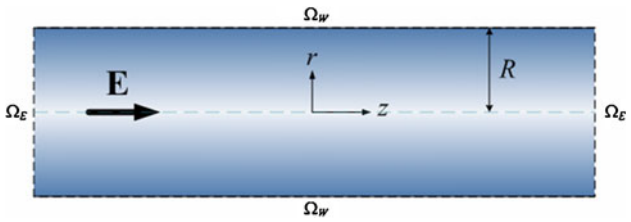

Fig. 1 Electrokinetic flow along the axis of a cylindrical nanochannel of radius R subject to an applied uniform electrical field **E** in the z direction; (r, z) are the computation domain of the cylindrical coordinates adopted with the origin on the axis of the channel; Ω_W and Ω_E are the channel wall and the input and output surfaces of that domain, respectively

R subject to an applied uniform electrical field **E**. The cylindrical coordinates r, θ, z are adopted with the origin on the axis of the channel. Because the present problem is θ symmetric, only the (r, z) domain needs be considered. Let Ω_W and Ω_E be the channel wall and the input and output surfaces of the computation domain, respectively.

We assume that the system under consideration is at a pseudo-steady state, the liquid phase is an incompressible Newtonian fluid containing N kinds of ionic species, the flow field is in the creeping flow regime, the channel surface is nonslip and nonconducting. In addition, **E** is relatively weak compared with the electrical field established by the channel wall, and the channel is sufficiently long so that the possible ion concentration polarization and nonuniform electric field arising from the selective transport of ions occurring at both ends of the channel is unimportant.

The channel wall is charged due to the dissociation/association of the functional group AH: $AH \Leftrightarrow A^- + H^+$ and $AH + H^+ \Leftrightarrow AH_2^+$. The corresponding equilibrium constants, K_a and K_b, can be expressed as $K_a = N_{A^-}[H^+]/N_{AH}$ and $K_b = N_{AH_2^+}/N_{AH}[H^+]$, with N_{A^-}, $N_{AH_2^+}$, N_{AH}, and $[H^+]$ being the surface densities of A^-, AH_2^+, and AH (mol/m^2), and the molar concentration of H^+, respectively. If we let N_{total} be the total density of AH, then $N_{total} = N_{A^-} + N_{AH} + N_{AH_2^+}$. It can be shown that the surface charge density, σ_s, is

$$\sigma_s = -FN_{total}\left(\frac{K_a - K_b[H^+]_s^2}{K_b[H^+]_s^2 + [H^+]_s + K_a}\right), \quad (1)$$

where $[H^+]_s$ and F are the value of $[H^+]$ on Ω_W and Faraday constant, respectively. For convenience, we define the scaled surface charge density $\sigma_s^* = \sigma_s eR/\varepsilon k_B T$, where e, ε, k_B, and T are the elementary charge, the permittivity of the liquid phase, Boltzmann constant, and the absolute temperature, respectively.

A perturbation approach similar to that of O'Brien and White (1978) and Ohshima (1995, 2006) is adopted to solve the present problem. The dependent variables, the

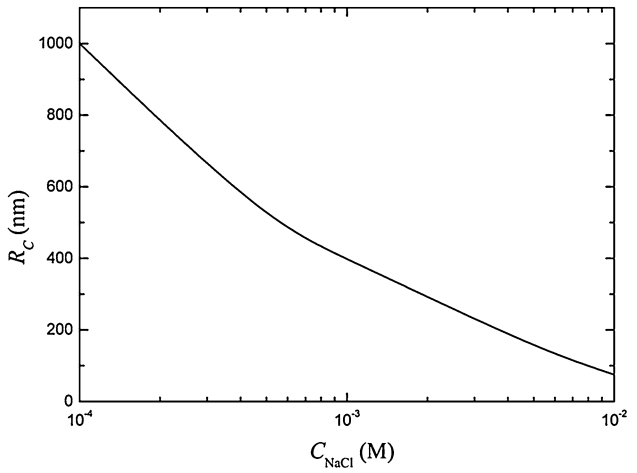

Fig. 2 Variation of the critical radius R_c with the background salt concentration C_{NaCl} at pH 7 and $N_{total} = 10^{-5}$ mol/m^2

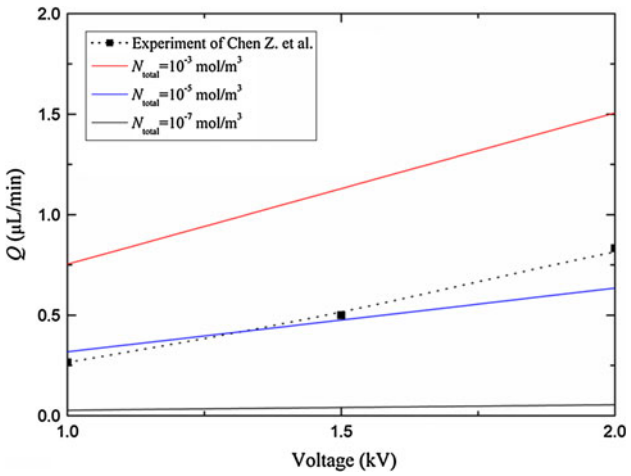

Fig. 3 Variations of the volumetric flow rate Q with applied voltage for various values of N_{total} at $R = 50$ μm, $C_{NaCl} = 4.5 \times 10^{-3}$ M, and pH 7. *Curves*, rescaled result from $R = 500$ nm; *dashed curve* with *square symbol*, experiment data of Chen et al. (2005)

electrical potential ϕ, the number concentration of the jth ionic species n_j, and the fluid velocity $\mathbf{v}$, are all partitioned into an equilibrium component and a perturbed component. The former (latter) is the value of that variable when $\mathbf{E}$ is absent (present). We assume that the channel is sufficiently long so that the end effect is negligible. Then, it can be shown that the present problem can be described by the following scaled equations and boundary conditions:

$$\nabla^{*2}\phi_e = \frac{(kR)^2}{\sum_{j=1}^{N}\alpha_{21}}\sum_{j=1}^{N}\alpha_{11}\exp\left(-\alpha_{10}\phi_e^*\right) \tag{2}$$

$$\nabla^{*2}\delta\phi^* = 0 \tag{3}$$

$$\eta\nabla^{*2}\mathbf{v}^* + \nabla^{*2}\phi_e^*\nabla^*\delta\phi^* = \mathbf{0} \tag{4}$$

$$\nabla^*\cdot\mathbf{v}^* = 0 \tag{5}$$

$$n_j^* = \exp\left(-\alpha_{10}\phi_e^*\right), \quad j = 1, 2, \ldots, N \tag{6}$$

$$\mathbf{n}\cdot\nabla^*\phi_e^* = -\sigma_s^* \text{ on } \Omega_W \tag{7}$$

$$\mathbf{n}\cdot\nabla^*\delta\phi^* = 0 \text{ on } \Omega_W \tag{8}$$

$$\mathbf{n}\cdot\nabla^*\phi_e^* = 0 \text{ on } \Omega_E \tag{9}$$

$$\mathbf{n}\cdot\nabla^*\delta\phi^* = -E_z^* \text{ on } \Omega_E \tag{10}$$

$$\mathbf{v}^* = \mathbf{0} \text{ on } \Omega_W \tag{11}$$

$$\mathbf{n}\cdot\nabla^*\mathbf{v}^* = 0 \text{ on } \Omega_E \tag{12}$$

Here, the subscript e and the prefix δ denote the equilibrium and the perturbed properties, respectively. $\mathbf{n}$ is the unit normal vector pointing into the system. $\nabla^* = R\nabla$ and $\nabla^{*2} = R^2\nabla^2$ are the scaled gradient operator and the scaled Laplace operator, respectively; $\kappa = \left[\sum_{j=1}^{N} n_{j0}(ez_j)^2/\varepsilon k_B T\right]^{1/2}$ is the reciprocal Debye screening length; z_j is the valence of ionic species $j, j = 1, 2, \ldots, N$; $n_j^* = n_j/n_{j0}$ with n_{j0} being the bulk ionic concentration of ionic species j; η is the fluid viscosity; $\mathbf{v}^* = \mathbf{v}/U^0$ with $U^0 = \varepsilon\zeta_a^2/R\eta$ being a reference velocity. $E_z^* = E_z/(\zeta_a/R)$, $\phi_e^* = \phi_e/\zeta_a$ and $\delta\phi^* = \delta\phi/\zeta_a$, where ζ_a ($=k_BT/z_1e$) is the thermal potential with z_1 being a reference ionic species. The parameter $\alpha_{\beta\gamma} = z_j^\beta n_{j0}^\gamma/z_1^\beta n_{10}^\gamma$ denotes the relative concentration of ionic species j relative to $[H^+]$. As suggested by Eq. 4, no pressure gradient is applied. Because $\mathbf{E}$ is weak relative to the electric field established by the channel, concentration polarization is unimportant, $\delta n_j^* = 0$, so is $\nabla^{*2}\delta\phi^* = 0$ in Eq. 8, and the ionic concentration follows Boltzmann distribution in Eq. 6.

Once the velocity profile is known, the scaled volumetric flow rate, $Q^* = Q/(\varepsilon\zeta_a^2 R/\eta)$, with Q being the volumetric flow rate can be evaluated by

$$Q^* = \iint_{S^*} (\mathbf{n}\cdot\mathbf{v}^*)\mathrm{d}S^* \text{ on } \Omega_E, \tag{13}$$

where $S^* = S/R^2$ is the scaled cross-sectional area of the channel.

3 Results and discussion

The present boundary-value problem is solved numerically by FlexPDE (version 2.22; PDE Solutions, Spokane Valley, WA, 2000), which was found to be sufficiently efficient and accurate for similar problems (Hsu et al. 2004a, b). Typically, using a total of ca. 15,384 and 12,948 nodes is sufficient for the resolution of the electric and the flow fields, respectively. An error limit of 10^{-5} is specified for both the electric potential and the flow velocity. For illustration, we assume that the background salt is NaCl,

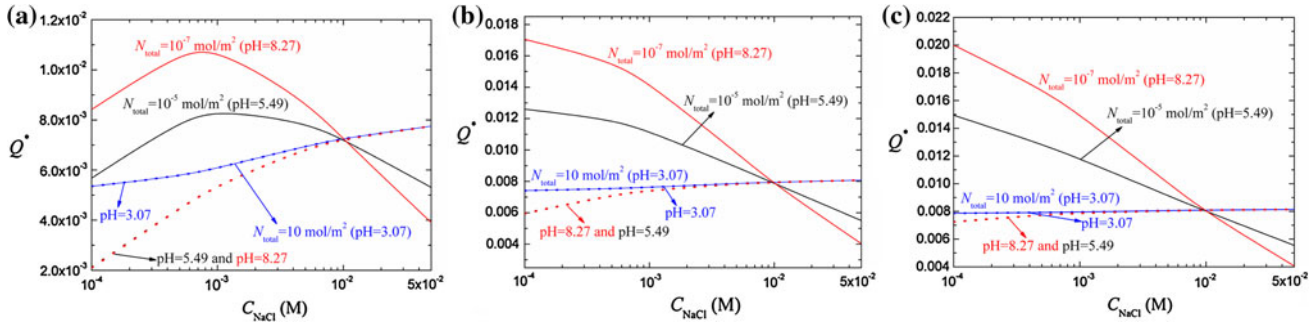

Fig. 4 Variations of the scaled volumetric flow rate Q^* with background salt concentration C_{NaCl} at various combinations of N_{total} and pH at $R = 50$ nm (**a**), $R = 200$ nm (**b**), $R = 500$ nm (**c**). *Solid curves*, charge-regulated channel; *dotted curves*, $\phi_s^* = -1.3022$

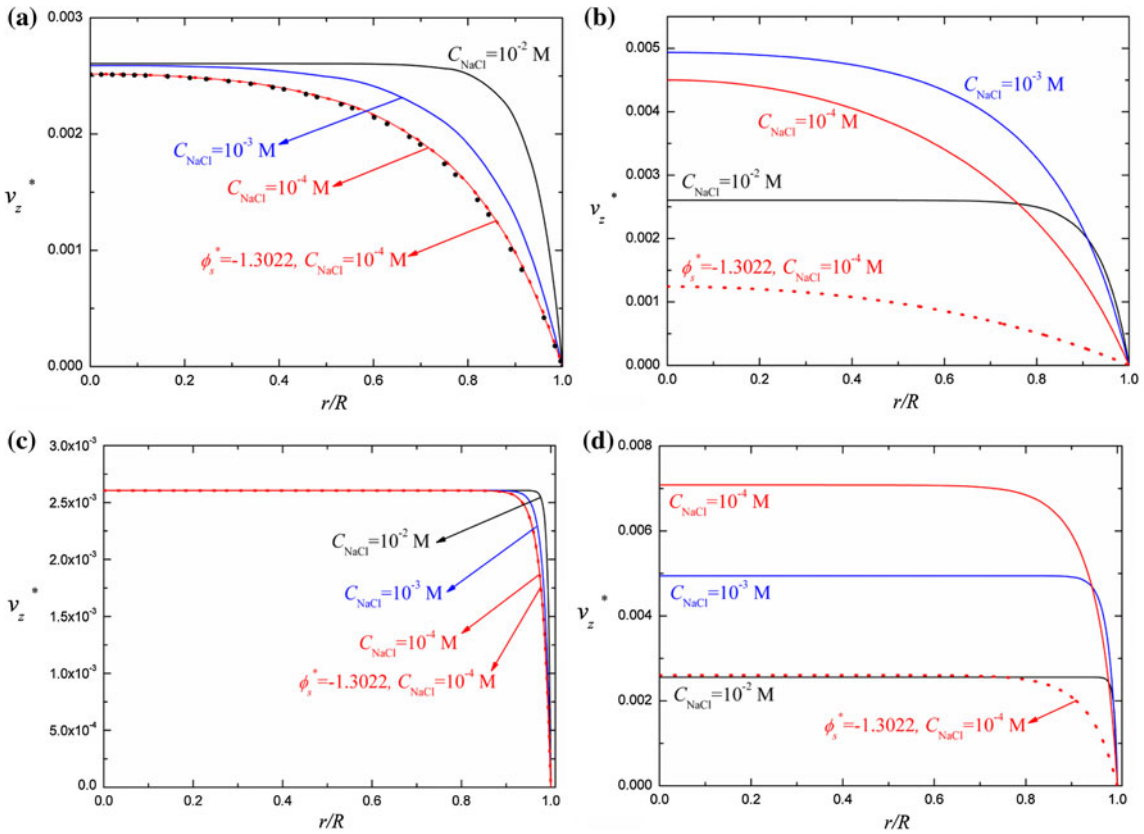

Fig. 5 Radial distribution of v_z^* for various values of C_{NaCl} in Fig. 4a at $N_{total} = 10$ mol/m^2 (**a**), $N_{total} = 10^{-7}$ mol/m^2 (**b**), $N_{total} = 10$ mol/m^2 in Fig. 4c (**c**), $N_{total} = 10^{-7}$ mol/m^2 (**d**). *Red dotted curves*, $\phi_s^* = -1.3022$ and $C_{NaCl} = 10^{-4}$ M; *black dotted curves*, analytical solution for $\phi_s^* = -1.3022$ and $C_{NaCl} = 10^{-4}$ M

and the solution pH is adjusted by HCl and NaOH, so that four kinds of ionic species need be considered: Na^+, Cl^-, H^+, and OH^-. The concentrations of these ionic species should satisfy that for $pH < pK_W/2$, $[H^+]_0 = 10^{-pH}$, $[Na^+]_0 = C_{NaCl}$, $[Cl^-]_0 = C_{NaCl} + 10^{-pH} - 10^{-(pK_W-pH)}$, and $[OH^-]_0 = 10^{-(pK_W-pH)}$, and for $pH < pK_W/2$, $[H^+]_0 = 10^{-pH}$, $[Na^+]_0 = C_{NaCl} + 10^{-(pK_W-pH)} - 10^{-pH}$, $[Cl^-]_0 = C_{NaCl}$, and $[OH^-]_0 = 10^{-(pK_W-pH)}$.

3.1 Influence of channel scale

To distinguish the flow in a nano-scaled channel and that in a larger-scaled one, we define a critical radius R_c, where $Q^* \propto (S^*)^n$ for $R_c < R$ with $n = 1 \pm 0.02$. $(R - R_c)$ is a measure for the part of a channel in which the volumetric flow rate is linearly proportional to its cross-sectional area. As seen in Fig. 2, R_c decreases with increasing background NaCl

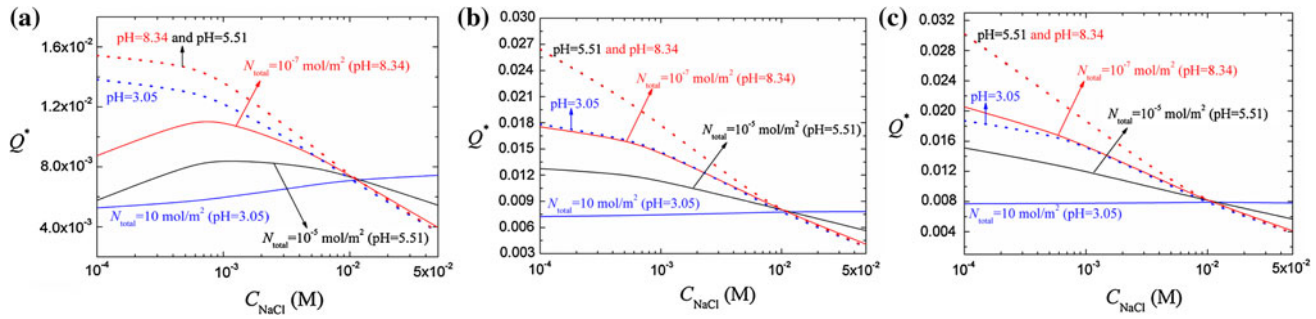

Fig. 6 Variations of Q^* with C_{NaCl} at various combinations of N_{total}, pH, and R. **a** $R = 50$ nm, **b** $R = 200$ nm, **c** $R = 500$ nm. *Solid curves*, charge-regulated surface; *dotted curves*, $\sigma_s^* = -22.61$

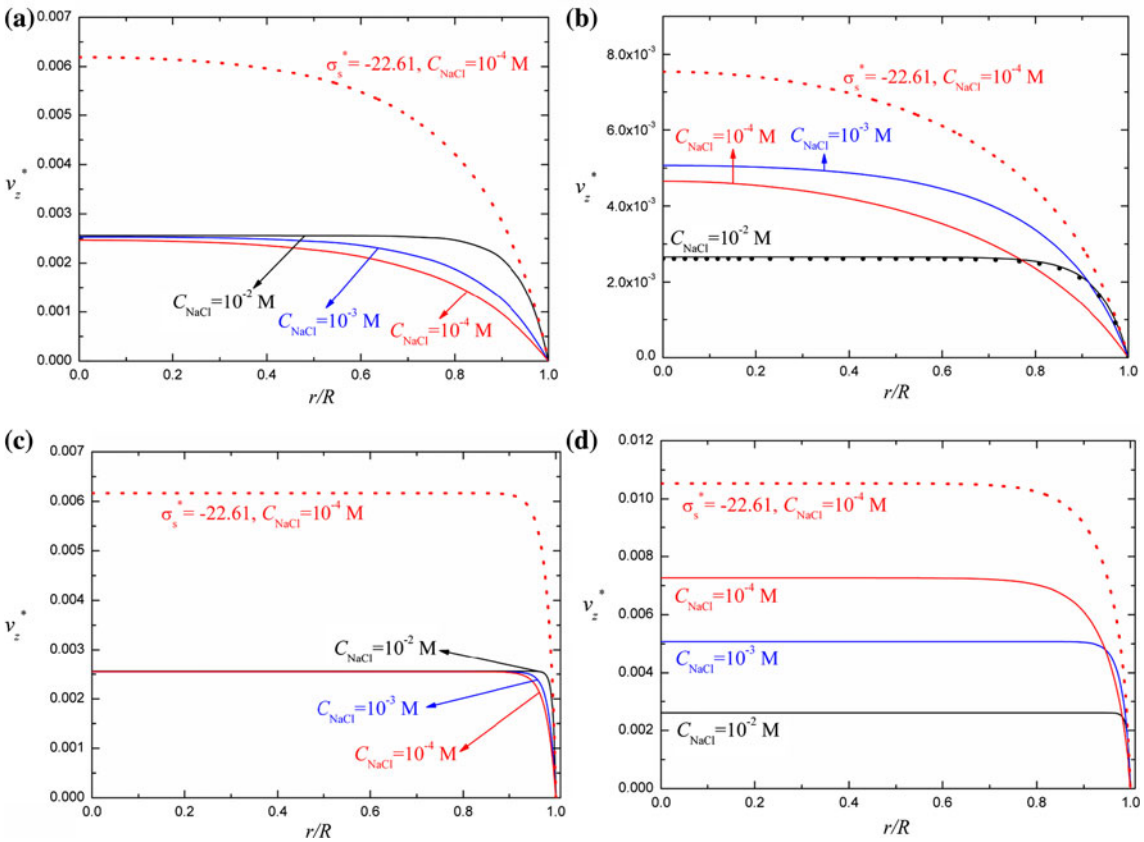

Fig. 7 Distributions of the scaled velocity v_z^* for various values of C_{NaCl} in Fig. 6a at $N_{total} = 10$ mol/m^2 (**a**), $N_{total} = 10^{-7}$ mol/m^2 (**b**), that in Fig. 6c at $N_{total} = 10$ mol/m^2 (**c**), $N_{total} = 10^{-7}$ mol/m^2 (**d**). *Red dotted curves*: $\sigma_s^* = -22.61$ and $C_{NaCl} = 10^{-4}$ M; *black dotted curves* in **b**: analytical solution for $\sigma_s^* = -22.61$ and $C_{NaCl} = 10^{-2}$ M (Chu and Ng 2012)

concentration, C_{NaCl}, in general. This is because the higher the C_{NaCl} the thinner the EDL. If C_{NaCl} is high, EDL is much thinner than channel radius so that the volumetric flow rate is proportional to its cross-sectional area. On the other hand, if C_{NaCl} is low, the EDL thickness can be comparable to the channel radius, yielding a large R_c. Note that the slope of the curve in Fig. 2 changes appreciably at $C_{NaCl} \cong 8 \times 10^{-4}$ M, suggesting that it is the critical level under the conditions assumed. We conclude that the flow behavior in a nano-scaled channel is more complicated than that in a larger-scaled one, where the flow rate is essentially proportional to its cross-sectional area (Chen et al. 2005).

3.2 Model verification by experimental data

The applicability of the present model is examined by fitting it to the experimental data of Chen et al. (2005), where an EDTA electrolyte solution of bulk conductance

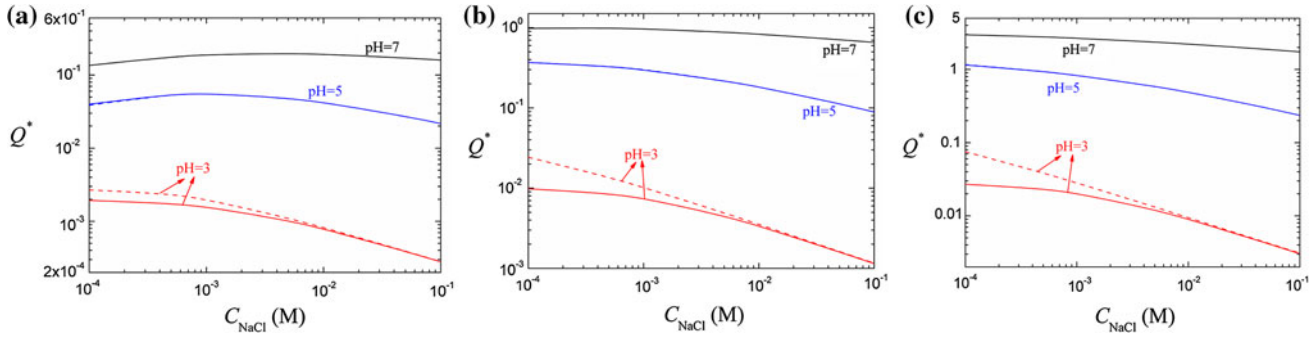

Fig. 8 Variations of Q^* with C_{NaCl} at various combinations of pH and R at $N_{total} = 10^{-5}$ mol/m^2; **a** $R = 50$ nm, **b** $R = 200$ nm, **c** $R = 500$ nm. *Solid curves*, four kinds of ions are considered; *dashed curves*, only two kinds of ions are considered

5×10^{-4} S/cm was used and the channel surface has silanol functional groups. To simulate their conditions, we assume $pK_a = 7$, $pK_b = 2$, and $C_{NaCl} = 4.5 \times 10^{-3}$ M. In this case, because R_c is smaller than 200 nm, Q can be rescaled by $Q(R = 500\ \text{nm})$; that is, $Q(R = 500\ \text{nm}) = Q(R = 200\ \text{nm}) \times (500^2/200^2)$.

Figure 3 illustrates the variations of the volumetric flow rate Q (μL/min) with applied electrical potential at various values of N_{total}. Here, Q is seen to increase linearly with the applied electrical potential, and the larger the N_{total} the larger the Q. According to the experimental data, $N_{total} \cong 10^{-5}$ mol/m^2, which is typical to a fused silica surface (Kirby and Hasselbrink 2004; Dolnik 2004).

3.3 Effect of the charged conditions

Let us examine first the effect of the charged conditions on the channel surface. Three cases are considered: a charge-regulated channel, a channel of constant charge density, and a constant electrical potential channel. It is known that the latter two models are the limiting cases of the first one. Figure 4 summarizes the variations in the scaled volumetric flow rate Q^* with C_{NaCl} for various combinations of N_{total}, pH, and R. For illustration, we assume $E = 5$ kV/m. Comparison is made between the behavior of a charge-regulated surface and a constant electrical potential surface. In the latter, the scaled electrical potential on the channel surface, $\phi_S^* = (\phi_S/\zeta_a)$ is fixed at -1.3022 when $C_{NaCl} = 10^{-2}$ M. Note that even ϕ_S^* is fixed, pH still varies with N_{total}. Therefore, the solid curves (charge-regulated) should be compared with the dotted curves (constant potential) at the same pH so that the EDL thickness is consistent.

Figure 4 shows that if N_{total} is sufficiently high (10 mol/m^2), the Q^* of a constant potential channel is essentially the same as that of a charge-regulated channel. However, if N_{total} is low, the behaviors of the two become different significantly. Their results have also been observed by Hsu et al. (2004a). The qualitative behavior of Q^* at $R = 50$ nm (Fig. 4a) is seen to be different from that at $R = 200$ and 500 nm (Fig. 4b, c). For example, if N_{total} is high (10 mol/m^2), the variation in Q^* at $R = 50$ nm is much more sensitive to that at $R = 200$ and 500 nm. This results from a rapid change in the EDL thickness/channel radius ratio. In addition, at $R = 50$ nm, if N_{total} is low (10^{-5} and 10^{-7} mol/m^2), Q^* shows a local maximum as C_{NaCl} varies, which is not seen at $R = 200$ and 500 nm. A comparison between Fig. 5a ($R = 50$ nm) and c ($R = 500$ nm) reveals that the variation of v_z^* with C_{NaCl} in the former is more appreciable than that in the latter, which explains the behavior of Q^* seen in Fig. 4a, c. Because the behavior of Q^* as C_{NaCl} varies depends on both v_z^* and ϕ_S^*, it is more complicated than that of v_z^*.

Figure 5d shows that v_z^* increases with decreasing C_{NaCl}, and Q^* decreases monotonically with C_{NaCl}; the former results from that the surface potential increases with EDL thickness. However, as the boundary of EDL reaches the center of the channel, a further increase in its thickness might not yield a faster electrokinetic velocity. For example, as seen in Fig. 5a, c, as C_{NaCl} decreases from 10^{-3} to 10^{-4} M, v_z^* decreases accordingly because the rate of increase in v_z^* is slower than that in EDL thickness. On the other hand, if C_{NaCl} exceeds ca. 10^{-3} M, because ϕ_S^* dominates, Q^* decreases with increasing C_{NaCl}, as seen in Fig. 4a. Figure 5b, d reveals that if N_{total} is low (10^{-7} mol/m^2), the behavior of v_z^* for a charge-regulated channel is different from that for a constant potential channel. On the other hand, if N_{total} is high (10 mol/m^2), the behavior of v_z^* for a charge-regulated channel is essentially the same as that for a constant potential channel even C_{NaCl} is lowered to 10^{-4} M, as seen in Fig. 5a, c. Note that the result at $C_{NaCl} = 10^{-4}$ M and $\phi_s^* = -1.3022$ in Fig. 5a is close to the analytical result of Hsu et al. (2004b), which also validates the present model.

Figure 6 summarizes the variations of Q^* with C_{NaCl} at various combinations of N_{total}, pH, and R. Both the results for a charge-regulated channel and a channel with fixed charge density are presented. In the latter, the scaled charge density σ_s^* is fixed at -22.61 (based on $C_{NaCl} = 10^{-2}$ M). Note that, to achieve this, pH needs be adjusted as N_{total} varies.

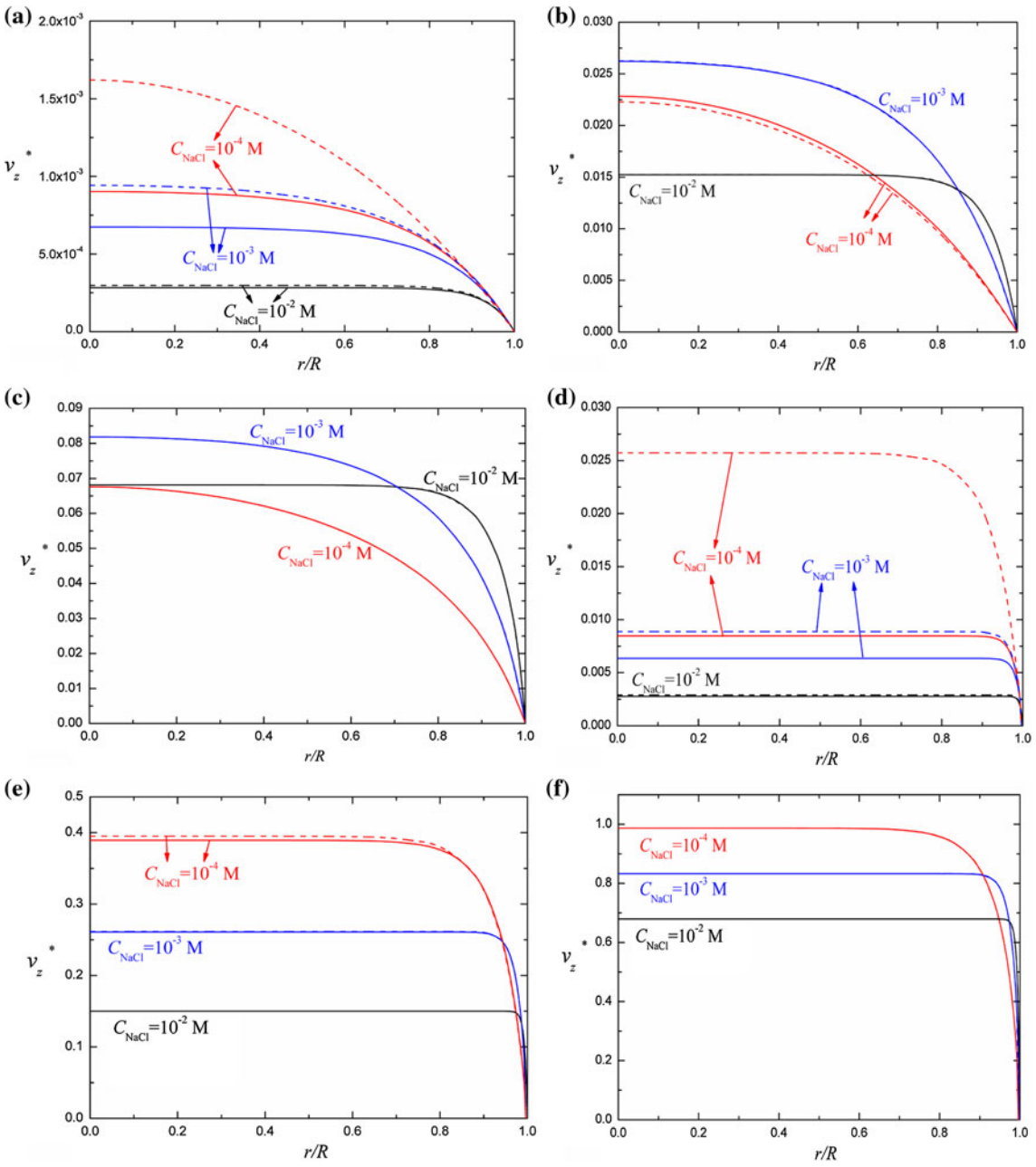

Fig. 9 Distributions of the scaled radial velocity v_z^* for various values of C_{NaCl} in Fig. 8a at pH 3 (**a**), pH 5 (**b**), pH 7 (**c**), that in Fig. 8c at pH 3 (**d**), pH 5 (**e**), pH 7 (**f**). *Solid curves*, four kinds of ions are considered; *dashed curves*, only two kinds of ions are considered

Figure 6 indicates that, in general, the lower the N_{total} and/or the higher the C_{NaCl} the closer the result of a charge-regulated channel to that of a channel of constant charge density. As seen in Fig. 6a, if N_{total} is sufficiently low (e.g., 10^{-7} mol/m^2), the qualitative behavior of Q^* for the two types of channels at low C_{NaCl} is quite different: One decreases monotonically with increasing C_{NaCl}, and the other has a local maximum. This is because the rate of increase in ϕ_s with decreasing C_{NaCl} for a charge-regulated channel is slower than that for a channel of constant charge density. Note that a charge-regulated channel is of feedback nature: As its surface potential gets high, H^+ is driven toward it so that the degree of dissociation of acidic functional group decreases, thereby reducing the surface potential. As mentioned previously, because the rate of increase in ϕ_s as C_{NaCl} decreases is faster than that in the EDL thickness, the Q^* for the case of a channel of constant charge density increases monotonically, instead of having a local maximum as in the case of a charge-regulated channel. Figure 6 also suggests that, in general, the larger

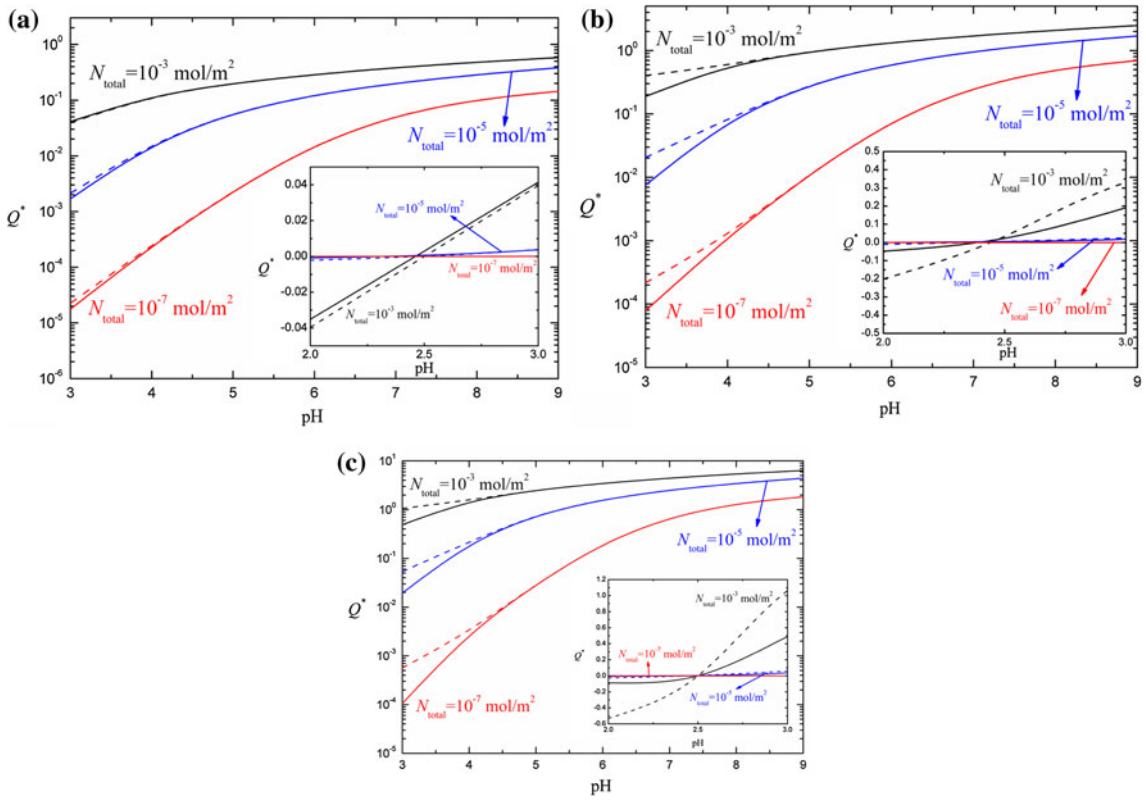

Fig. 10 Variations of Q^* with pH at various combinations of N_{total} and R at $C_{NaCl} = 10^{-3}$ M; **a** $R = 50$ nm, **b** $R = 200$ nm, **c** $R = 500$ nm. *Solid curves*, four kinds of ions are considered; *dashed curves*, only two kinds of ions are considered

the R the closer the results for a channel of constant charge density to those for a charge-regulated channel.

It is interesting to note that at high N_{total} (10 mol/m^2), Q^* increases with C_{NaCl}, which is different from the behavior of Q^* at low N_{total} and that for the case of a channel of constant charge density. As can be seen in Fig. 7a, where N_{total} is significantly high (10 mol/m^2), and if C_{NaCl} is low (10^{-4} M), the v_z^* for a charge-regulated channel differ significantly from that for a channel of constant charge density. Figure 7b, d shows that if N_{total} is low (10^{-7} mol/m^2), the v_z^* of a charge-regulated channel is similar to that of a channel of constant charge density, except that the latter overestimates v_z^*, which arises from that the rates of increase in ϕ_s of the two channels as C_{NaCl} varies are different significantly. The v_z^* for the case where $N_{total} = 10^{-7}$ mol/m^2, $C_{NaCl} = 10^{-2}$ M, and $R = 50$ in Fig. 7b is essentially the same as the corresponding analytical result (Chu and Ng 2012), which also validates the present model.

3.4 Influence of pH, N_{total}, and C_{NaCl}

Let us examine next the influences of pH, N_{total}, and C_{NaCl} on the electrokinetic behavior in a charge-regulated channel. As seen in Fig. 8, where $E = 10$ kV/m, at a higher pH, because the dissociation of H^+ from the channel surface is more complete, ϕ_s is higher and, therefore, the electrokinetic velocity is faster and Q^* is larger.

Figure 8a ($R = 50$ nm) shows that for both pH 5 and 7, Q^* has a local maximum as C_{NaCl} varies. As mentioned previously, this results from that the EDL thickness is close to the channel radius. As can be seen in Fig. 8, if both pH and C_{NaCl} are low, assuming the presence of two types of ions only might yield an appreciable deviation in Q^*. This is because the presence of H^+ is significant in this case. The types of ionic species in the liquid phase influence the EDL thickness, and therefore ϕ_s and Q^*. In general, Q^* is overestimated when only two kinds of ions are considered because the EDL in this case is thicker than that in the case where the other two kinds of ions are also considered. In other words, ϕ_s, and therefore, v_z^*, is overestimated when only two kinds of ions are considered. However, as seen in Fig. 9a, d, the deviation in v_z^* due to ignoring the other two kinds of ions decreases with increasing C_{NaCl}. This is expected because the higher the C_{NaCl} the more significant the presence of Na^+ and Cl^-. As illustrated in Figs. 8 and 9, at pH 5 and 7, because H^+ and OH^- are relatively unimportant, the v_z^* and Q^* for the case of four kinds of ions are close to those for the case of two kinds of ions. It is interesting to see in Fig. 8a (Fig. 9b) that at pH 5 and low

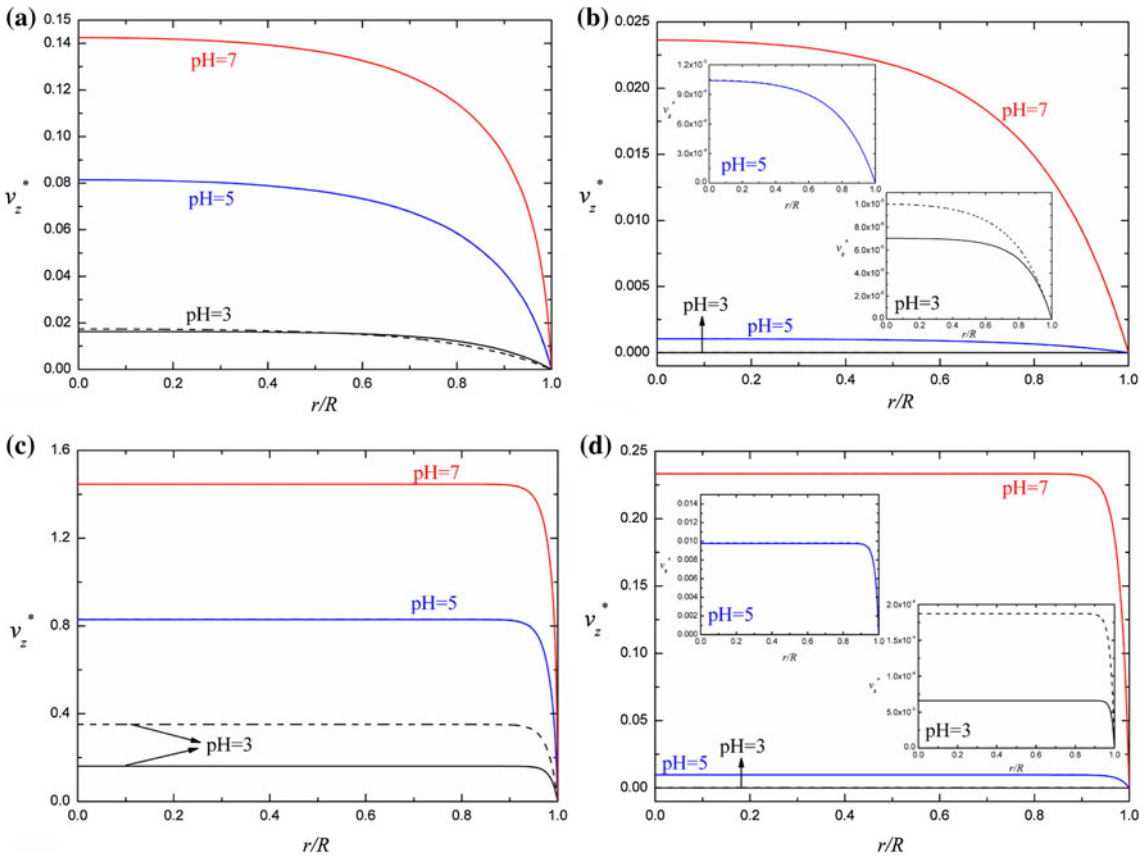

Fig. 11 Distributions of the scaled radial velocity v_z^* for various values of pH for the case of Fig. 10a at $N_{\text{total}} = 10^{-3}$ mol/m^2 (**a**), $N_{\text{total}} = 10^{-7}$ mol/m^2 (**b**), that in Fig. 10c at $N_{\text{total}} = 10^{-3}$ mol/m^2 (**c**), $N_{\text{total}} = 10^{-7}$ mol/m^2 (**d**). *Solid curves* four kinds of ions are present; *dashed curves*, only two kinds of ions are present

C_{NaCl}, considering only two kinds of ions will underestimate Q^* (v_z^*). This is because that although ϕ_s is overestimated when only two kinds of ions are considered, so is the EDL thickness, making Q^* (v_z^*) underestimated, especially when EDL thickness is comparable to R.

The variations of Q^* with pH for various combinations of N_{total} and R are presented in Fig. 10, which shows that the qualitative behaviors of Q^* in all case considered are similar to each other. In general, Q^* increases with increasing pH and/or N_{total}, which results from the increase in the density of negatively charged functional groups on the channel surface.

The rate of increase in Q^* with increasing pH at lower N_{total} is faster than that at higher N_{total} because the rate of increase in the density of the charged functional group in the former is faster. This can be explained by Fig. 11a, b that although the qualitative behavior of v_z^* at $N_{\text{total}} = 10^{-3}$ mol/m^2 is similar to that at $N_{\text{total}} = 10^{-7}$ mol/m^2 the order of difference in v_z^* for various pH values in the latter is significantly larger than that in the former. Figure 10 reveals that neglecting the presence of H^+ and OH^- can be appreciable at low pH values. In addition, consider only two kinds of ions will overestimate Q^*, and the larger the channel the more serious the deviation. Note that the direction of electroosmotic flow is reversed for pH lower than 2.5, the point of zero charge. In this case, the channel surface becomes positively charged. This nature of a charge-regulated channel can be applied, for example, to the separation of nano-sized entities.

Figure 11 indicates that the larger the channel the more serious the deviation in v_z^* due to the consideration of two kinds of ions only. As mentioned previously, this arises from that the competition between the effect of EDL thickness and that of surface potential is more significant in small-sized channels.

4 Conclusions

The electrokinetic flow in a charge-regulated channel is investigated taking account of the presence of multiple ionic species so that the model considered is closer to reality than previous models. Adopting a channel with its surface bearing silanol functional groups ($pK_a = 7$, $pK_b = 2$) and NaCl salt

solution of molar concentration C_{NaCl} and its pH adjusted by HCl and NaOH as an example, the velocity distribution and the volumetric flow rate under various conditions are examined. The results gathered can be summarized as following. (1) The critical channel radius, the radius that the volumetric flow rate is linearly proportional to the cross-sectional area of a channel, increases with C_{NaCl}; the plug flow assumption in a micron-scaled channel becomes invalid in a nano-scaled one. (2) As the density of the functional groups on the surface of a charge-regulated channel, N_{total}, increases (decreases), it approaches a constant potential (charge density) channel. If N_{total} is low, the behavior of a charge-regulated channel is similar to that of a channel of constant charge density at high C_{NaCl} (e.g., 10^{-2} M) and large channel radius (e.g., 200 nm). The volumetric flow rate of a small channel (e.g., 50 nm) has a local maximum as C_{NaCl} varies, which is not seen in a constant potential channel or a channel of charge density. The presence of the local maximum results from the competition between the effect of electric double layer thickness and that of channel surface potential. (3) Both the velocity and the volumetric flow rate are overestimated in most cases when only two kinds of ionic species are considered. This results from the underestimation of the electric double layer thickness at a low pH. If pH is close to 7, Na^+ and Cl^- dominate, and the presence of other ionic species can be neglected. (4) The volumetric flow rate is more sensitive to the variation in pH when N_{total} is low, and the positive deviation of that quantity due to the consideration of two kinds of ions only is more serious at large channel radius. (5) The direction of electrokinetic flow can be regulated by pH, which has potential applications in, for example, separation of colloidal particles.

References

Ai Y, Liu J, Zhang BK, Qian S (2010) Field effect regulation of DNA translocation through a nanopore. Anal Chem 82:8217–8225

Campbell LC, Wilkinson MJ, Manz A, Camilleri P, Humphreys CJ (2004) Electrophoretic manipulation of single DNA molecules in nanofabricated capillaries. Lab Chip 4:225–229

Cao QQ, Zuo CC, Li LJ, Ma YH, Li N (2010) Electroosmotic flow in a nanofluidic channel coated with neutral polymers. Microfluid Nanofluid 9:1051–1062

Chen Z, Ping Wang, Chang HC (2005) An electro-osmotic micropump based on monolithic silica for micro-flow analyses and electro-sprays. Anal Bioanal Chem 382:817–824

Chu HCW, Ng CO (2012) Electroosmotic flow through a circular tube with slip–stick striped wall. J Fluids Eng 134:111201

Daiguji H, Yang PD, Majumdar A (2004a) Ion transport in nanofluidic channels. Nano Lett 4:137–142

Daiguji H, Yang PD, Szeri AJ, Majumdar A (2004b) Electrochemomechanical energy conversion in nanofluidic channels. Nano Lett 4:2315–2321

Dolnik V (2004) Wall coating for capillary electrophoresis on microchips. Electrophoresis 25:3589–3601

Gasparac R, Kohli P, Mota MO, Trofin L, Martin CR (2004) Template synthesis of nano test tubes. Nano Lett 4:513–516

Hirst LS, Parker ER, Abu-Samah Z, Li Y, Pynn R, MacDonald NC, Safinya CR (2005) Microchannel systems in titanium and silicon for structural and mechanical studies of aligned protein self-assemblies. Langmuir 21:3910–3914

Hsu JP, Hung SH, Yu HY (2004a) Electrophoresis of a sphere at an arbitrary position in a spherical cavity filled with Carreau fluid. J Colloid Interface Sci 280:256–263

Hsu JP, Ku MH, Kao CY (2004b) Electrophoresis of a spherical particle along the axis of a cylindrical pore: effect of electro-osmotic flow. J Colloid Interface Sci 276:248–254

Hu K, Bard AJ (1997) Characterization of adsorption of sodium dodecyl sulfate on charge-regulated substrates by atomic force microscopy force measurements. Langmuir 13:5418–5425

Karenga S, El Rassi Z (2010) A novel, neutral hydroxylated octadecyl acrylate monolith with fast electroosmotic flow velocity and its application to the separation of various solutes including peptides and proteins in the absence of electrostatic interactions. Electrophoresis 31:3192–3199

Karnik R, Castelino K, Fan R, Yang P, Majumdar A (2005) Effects of biological reactions and modifications on conductance of nanofluidic channels. Nano Lett 5:1638–1642

Kim SJ, Wang YC, Lee JH, Jang H, Han J (2007) Concentration polarization and nonlinear electrokinetic flow near a nanofluidic channel. Phys Rev Lett 99:044501

Kirby BJ, Hasselbrink EF (2004) Zeta potential of microfluidic substrates: 1. Theory, experimental techniques, and effects on separations. Electrophoresis 25:187–202

Krapf D, Wu MY, Smeets RMM, Zandbergen HW, Dekker C, Lemay SG (2006) Fabrication and characterization of nanopore-based electrodes with radii down to 2 nm. Nano Lett 6:105–109

Li J, Stein D, McMullan C, Branton D, Aziz MJ, Golovchenko JA (2001) Ion-beam sculpting at nanometer length scales. Nature 412:166–169

Liu CC, Maciel GE (1996) The fumed silica surface: a study by NMR. J Am Chem Soc 118:5103–5119

Mao P, Han J (2005) Fabrication and characterization of 20 nm planar nanofluidic channels by glass–glass and glass–silicon bonding. Lab Chip 5:837–844

Mei J, Xu JR, Xiao YX, Liao XY, Qiu GF, Feng YQ (2008) A novel covalent coupling method for coating of capillaries with liposomes in capillary electrophoresis. Electrophoresis 29:3825–3833

Nawrocki J (1997) The silanol group and its role in liquid chromatography. J Chromatogr A 779:29–71

Nischang I, Chen G, Tallarek U (2006) Electrohydrodynamics in hierarchically structured monolithic and particulate fixed beds. J Chromatogr A 1109:32–50

O'Brien RW, White LR (1978) Electrophoretic mobility of a spherical colloidal particle. J Chem Soc Faraday Trans 2 74:1607–1626

Ohshima H (1995) Electrophoresis of soft particles. Adv Colloid Interface Sci 62:189–235

Ohshima H (2006) Electrophoresis of soft particles: analytic approximations. Electrophoresis 27:526–533

Pennathur S, Santiago JG (2005) Electrokinetic transport in nanochannels. 1. Theory. Anal Chem 77:6772–6781

Pu QS, Yun JS, Temkin H, Liu SR (2004) Ion-enrichment and ion-depletion effect of nanochannel structures. Nano Lett 4:1099–1103

Qiao R, Aluru NR (2004) Charge inversion and flow reversal in a nanochannel electro-osmotic flow. Phys Rev Lett 92:198301

Qu WL, Li DQ (2000) A model for overlapped EDL fields. J Colloid Interface Sci 224:397–407

Schoch RB, Bertsch A, Renaud P (2006) pH-controlled diffusion of proteins with different pI values across a nanochannel on a chip. Nano Lett 6:543–547

Storm AJ, Chen JH, Ling XS, Zandbergen HW, Dekker C (2003) Fabrication of solid-state nanopores with single-nanometre precision. Nat Mater 2:537–540

Tas N, Berenschot J, Mela P, Jansen H, Elwenspoek M, van den Berg A (2002) 2D-confined nanochannels fabricated by conventional micromachining. Nano Lett 2:1031–1032

Thompson AP (2003) Nonequilibrium molecular dynamics simulation of electro-osmotic flow in a charged nanopore. J Chem Phys 119:7503–7511

van der Heyden FHJ, Stein D, Dekker C (2005) Streaming currents in a single nanofluidic channel. Phys Rev Lett 95:116104

Wang M, Liu J, Chen S (2007) Electric potential distribution in nanoscale electroosmosis: from molecules to continuum. Mol Simul 33:1273–1277

Wang XY, Wang SL, Gendhar B, Cheng C, Byun CK, Li GB, Zhao MP, Liu SR (2009) Electroosmotic pumps for microflow analysis. Trends Anal Chem 28:64–74

Wang M, Kang QJ, Ben-Naim E (2010) Modeling of electrokinetic transport in silica nanofluidic channels. Anal Chim Acta 664:158–164

White HS, Bund A (2008) Ion current rectification at nanopores in glass membranes. Langmuir 24:2212–2218

Yeh LH, Hsu JP, Qian S, Tseng SJ (2012a) Counterion condensation in pH-regulated polyelectrolytes. Electrochem Commun 19: 97–100

Yeh LH, Xue S, Joo SW, Qian S, Hsu JP (2012b) Field effect regulation of surface charge property and EOF in nanofluidics. J Phys Chem C 116:4209–4216

Yuan Z, Garcia AL, Lopez GP, Petsev DN (2007) Electrokinetic transport and separations in fluidic nanochannels. Electrophoresis 28:595–610